Nature of one-dimensional excitons in polysilanes

T. Hasegawa
Department of Pure and Applied Sciences, The University of Tokyo, Tokyo 153, Japan
and Department of Applied Physics, The University of Tokyo, Tokyo 113, Japan

Y. Iwasa
Japan Advanced Institute of Science and Technology (JAIST), Ishikawa 923-12, Japan
and Department of Applied Physics, The University of Tokyo, Tokyo 113, Japan

T. Koda
Department of Physical and Mathematical Sciences, Japan Women's University, Tokyo 112, Japan
and Department of Applied Physics, The University of Tokyo, Tokyo 113, Japan

H. Kishida
Department of Physics, The University of Tokyo, Tokyo 113, Japan
and Department of Applied Physics, The University of Tokyo, Tokyo 113, Japan

Y. Tokura
Department of Applied Physics, The University of Tokyo, Tokyo 113, Japan;
Department of Physics, The University of Tokyo, Tokyo 113, Japan;
and Joint Research Center for Atom Technology (JRCAT), Tsukuba 305, Japan

S. Wada and H. Tashiro
Photodynamics Research Center, Institute of Physical and Chemical Research (RIKEN), Sendai 980, Japan

H. Tachibana
Joint Research Center for Atom Technology (JRCAT), Tsukuba 305, Japan
and National Institute of Materials and Chemical Research, Tsukuba 305, Japan

M. Matsumoto
National Institute of Materials and Chemical Research, Tsukuba 305, Japan
(Received 2 May 1996; revised manuscript received 9 July 1996)

One-dimensional (1D) exciton states have been studied by nonlinear optical spectroscopy on organosilicon polymer polysilanes (PS's). From systematic variation of the linear and nonlinear optical spectra upon changing the backbone conformation, the following two characteristic exciton parameters have been evaluated; the ratio $|\chi^{(3)}|/\alpha$ of the modulus of third-order nonlinear optical susceptibility $|\chi^{(3)}|$ to the absorption coefficient α; and the energy difference ΔE_{12} between the lowest and second lowest exciton energies E_1 and E_2, which are theoretically related, respectively, to the Bohr radius and to the binding energy of excitons. It was found that $|\chi^{(3)}|/\alpha$ increases, whereas ΔE_{12} remains almost unchanged, with increasing valence and conduction-band widths. These features cannot be accounted for either by the Wannier- or Frenkel-type exciton model. From analysis by a unified 1D exciton model, it has been concluded that the 1D excitons in PS's represent a unique system having an intermediate character in between the Frenkel- and Wannier-exciton regimes, where the on-site Coulomb (or exchange) interactions play a crucial role in determining the characteristic exciton structures as observed. [S0163-1829(96)07639-4]

I. INTRODUCTION

In the past few years, concentrated interest has been focused on optical properties of quasi-one-dimensional (Q1D) semiconductor structures, mainly from an interest in materials showing large optical nonlinearities. Artificial quantum wires[1–3] as well as chemically synthesized conjugated polymers like polydiacetylenes (PDA's) or polyacetylenes[4–7] have received extensive experimental and theoretical investigations, whereby several notable features of Q1D excitons have been elucidated. Among these Q1D excitonic materials, organosilicon polymers [usually referred to as polysilanes PS's] have been attracting considerable interest, because the linear σ-bond chains in PS's are found to exhibit remarkable linear and nonlinear optical features which can be interpreted as due to the ''quantum wire structure'' effect. As compared with rather complicated low-dimensional quantum structures with use of inorganic semiconductor devices, PS's have several advantages, such as the availability of good film samples suitable for making detailed linear and nonlinear spectroscopy.[8–10]

A significant difference in the exciton effect in the Q1D semiconductors as compared with that in 2D or 3D semiconductors can be qualitatively understood in terms of the ''1D hydrogen-atom'' picture discussed by Loudon in the late 1950s.[11] In a perfect 1D system, the binding energy becomes infinite and the envelope-function approaches a δ function in the lowest ($\nu=1$) exciton state, due to the singularity of the Coulomb potential at the origin. [As for the higher exciton states ($\nu>1$), the energies are all doubly degenerate with respect to the inversion symmetry.] In actual Q1D semiconductors, however, such singularity must be more or less avoided, because of the contribution of non-1D effect in the actual system, and also due to the crude nature of the effective-mass approximation in the Wannier exciton regime. Nonetheless, it has been predicted that in such Q1D semiconductors, the lowest ($\nu=1$) exciton would have a very large binding energy, and that most of the oscillator strength would strongly concentrate on the lowest exciton state.[12–15] Because of such a peculiarity of the lowest exciton state in Q1D semiconductors, other dipole-allowed excited states, including both discrete higher excitons and the continuum states for free-electron-hole pairs, become practically unobservable in the linear absorption spectrum, which is in sharp contrast with the case of 3D and 2D semiconductors, where strong band-to-band transitions dominate the absorption spectra above the band-gap energy.

The predicted features of Q1D semiconductors have been found to be well realized in several conjugated polymers, in particular in σ-conjugated PS's. In agreement with these predictions, linear absorption spectra of PS's exhibit only a single absorption peak which is attributed to the lowest exciton state.[8–10] Moreover, from detailed nonlinear optical (NLO) studies by means of the third-harmonic generation (THG) measurement and other means of third-order NLO spectroscopy as well, the overall features of the 1D exciton structure have been elucidated in detail for one of the typical PS's, poly(di-*n*-hexylsilane) (PDHS), having an all-trans backbone conformation.[16,17] In the THG $|\chi^{(3)}|$ spectrum of PDHS, three distinct peaks have been observed, and they are identified as the multiphoton resonance structures associated with the lowest three ($\nu=1$, 2, and 3) 1D exciton states in the PS backbones. The energies of the lowest, the second, and the third excitons have been determined experimentally by one- and two-photon absorption measurements,[18,19] by THG,[20] and by electric-field-induced second-harmonic-generation (EFISHG) (Ref. 21) and electroabsorption (EA) measurements.[22]

Among these excitons, the third ($\nu=3$) exciton is dipole allowed, but is actually hidden from observation in the linear (one-photon) absorption spectrum, due to the characteristic exciton effect in the Q1D semiconductor as mentioned above. The observation of the third exciton just becomes possible by means of the THG $|\chi^{(3)}|$ measurements, due to the fact that the multiphoton nonlinear optical process includes the transitions between the higher exciton states, which have a significantly large dipole moment. This feature has been well explained by Abe, Schreiber, and Su in terms of a 1D exciton model,[23,24] where the 1D tight-binding model is supplemented by long-range Coulomb interactions.

Here we note that in the above 1D exciton model, Coulomb correlations are applied, only within the subspace of single electron-hole pair excitation for the formation of excitons in long chains of several hundred Si atoms. Conversely, for a theoretical treatment on similar but finite polyene molecules, double excitation configuration has been shown to be crucial to interpret the existence of their lower-lying optically forbidden ^{1}Ag excited state.[25,26] In infinite polymers like PS's, however, the above single excitation approximation may be fairly reasonable because the lower-lying ''covalent'' ^{1}Ag states, as observed in the finite polyene molecules, are pointed out, by Dixit, Guo, and Mazumdar,[27] to be irreverent to their nonlinear optical properties.

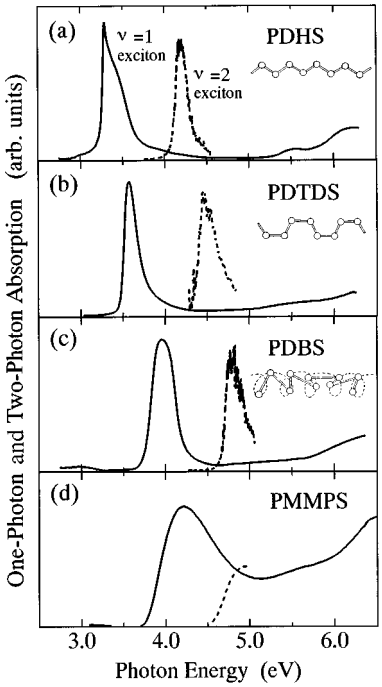

FIG. 1. One-photon absorption (solid curve) and two-photon absorption (dashed curve) spectra of PS's with four kinds of backbone conformations: (a) poly(di-*n*-hexylsilane) (PDHS) with all-trans conformation, (b) poly(di-*n*-tetradecylsilane) (PDTDS) with alternating trans-gauche conformation, (c) poly(di-*n*-butylsilane) (PDBS) with 7/3 helical conformation, and (d) poly(methyl-4-methylpentylsilane) (PMMPS) with disordered conformation. The lowest ($\nu=1$) and second ($\nu=2$) exciton energies depend on the backbone conformation.

A similar Q1D exciton picture is also expected to apply, not only for PDHS, but also for other Q1D PS's having various backbone conformations depending on the length of their alkylsubstituents,[28–30] as shown in the inset of Fig. 1. Such a variety in the conformation is attributable to the steric effect of the alkylsubstituents upon crystallization.[8] These backbone structures must have a significant influence upon the electronic band structures. Accordingly, one may be able to obtain information how the excitonic states are changed by the change in the backbone structure. Experimental data showing such a conformation effect in PS's are demonstrated in Fig. 1 for the one-photon absorption spectra (solid curve) of PS's with four kinds of backbone conformations. The respective backbone structures are schematically shown in the inset: (a) poly(di-*n*-hexylsilane) (PDHS: $R=R'=-C_6H_{13}$) with all-trans conformation, (b) poly(di-*n*-tetradecylsilane)

(PDTDS: $R=R'=-C_{14}H_{29}$) with trans-gauche conformation, (c) poly(di-*n*-butylsilane) (PDBS: $R=R'=-C_4H_9$) with 7/3 helical conformation, and (d) poly(methyl-4-methylpentylsilane) [PMMPS: $R=-CH_3$, $R=-(CH_2)_3-CH-(CH_3)_2$] with disordered conformation.[8] As seen in Fig. 1, a single and sharp exciton absorption peak due to the lowest exciton, observed at 3.32 eV for PDHS, are systematically shifted to 3.58 eV for PDTDS, to 3.95 eV for PDBS, and to 4.12 eV for PMMPS, in the order of decreasing symmetry in the backbone conformation, providing a unique opportunity for the study of Q1D excitons under systematic change in the relevant band parameters.

In the previous studies, two-photon and electroabsorption spectra have been reported for the same four kinds of PS's, thereby revealing the common features inherent to the Q1D exciton states in these systems.[28–30] In this study, we put emphasis on the systematic trend of the characteristic exciton states in PS's caused by the change in the backbone conformation. Simultaneous measurements were made on the THG $|\chi^{(3)}|$ spectra, the one- and two-photon absorption spectra, on these four PS's in the form of spin-cast films over a wide range of fundamental photon energy at room temperature. The results are represented by two useful parameters, $|\chi^{(3)}|/\alpha$, the ratio of $|\chi^{(3)}|$ and the absorption coefficient α, and the difference ΔE_{12} between the lowest and the second lowest exciton energies, $\Delta E_{12}=E_2-E_1$, obtained from linear and nonlinear optical spectra. The backbone conformation dependence of these parameters is analyzed by theoretical calculation based on the 1D exciton model.

II. EXPERIMENT

Four kinds of PS's with different length of alkylsubstituents[28–30] were used in this study. Powder material of respective PS's was synthesized chemically by reductive coupling of corresponding dialkyldichrolosilanes using 18-crown-6 as a phase catalyst. Then the powders were dissolved in heptane, and the solution was spin casted onto synthetic fused silica plates. The film was dried at 380 K for 15 min and then kept at room temperature overnight, before using the film for optical measurements. This procedure is suited to crystallize the alkylsubstituents having four different types of backbone conformation.[28] The films obtained in this way were composed of randomly oriented polymers with an average of molecular weight of about 10^5.

The measurements of THG $|\chi^{(3)}|$ spectra, as well as one- and two-photon absorption spectra, were done on these film samples at room temperature, following the procedure described in detail in previous publications.[16–18,29] In the following, we summarize the results together with some remarks on the present THG measurements: In the present measurements, we evaluated the modulus $|\chi^{(3)}|$ of complex third-order NLO susceptibility $\chi^{(3)}(-3\omega;\omega,\omega,\omega)$ $[=|\chi^{(3)}|\exp(i\phi)]$. As an excitation source for THG, three kinds of tunable laser systems were adopted to cover fundamental photon energy in the range from 0.57 to 2.2 μm; pulsed dye lasers pumped with a Xe-Cl excimer laser with 13 kinds of laser dyes were used for the range from 0.57 to 1.03 μm (from 2.15 to 1.20 eV in photon energy), a two-stage H_2 Raman shifting of a tunable dye laser[31] with four kinds of laser dyes was used in the range from 1.05 to 1.36 μm (from 1.18 to 0.91 eV), and a difference frequency generator using a $LiNbO_3$ crystal coupled with a Nd:YAG (yttrium aluminum garnet) laser and a dye laser with two kinds of laser dyes[32] was used to cover the range from 1.5 to 2.2 μm (from 0.82 to 0.56 eV).

TABLE I. Experimental values related to the exciton states in PS's (PDHS, PDTDS, PDBS, and PMMPS) with different backbone conformations.

	PDHS	PDTDS	PDBS	PMMPS
Lowest exciton energy: E_1 (eV)	3.32	3.58	3.95	4.12
second exciton energy: E_2 (eV)	4.19	4.45	4.76	
Energy difference E_2-E_1 (eV)	0.87	0.87	0.81	
$\lvert\chi^{(3)}\rvert$ at peak (10^{-20} m^2/V^2)	12.9 (at 1.09 eV)	9.45 (at 1.18 eV)	8.6 (at 1.31 eV)	
α at peak (10^7 1/m)	1.9 (at 3.29 eV)	1.5 (at 3.58 eV)	2.5 (at 3.96 eV)	
$\lvert\chi^{(3)}\rvert/\alpha$ by fitting (10^{-27} m^3/V^2)	8.5	5.7	3.3	

The standard Maker-fringe method was employed to evaluate $|\chi^{(3)}|$ for the respective samples.[33] The sample was placed in a vacuum chamber placed upon a goniometer head. All measurements were done in a vacuum of $\sim 10^{-3}$ torr to avoid the contribution of the NLO effect of the air to the observed TH intensities. For a quantitative determination of third-order NLO susceptibility, we used synthetic fused silica plates (0.3 or 1.0 mm thick) as a standard material.[34] For the determination of the absolute value of $|\chi^{(3)}|$, the thickness of the film sample was measured with a stylus-type thickness meter.[35] The values of the $|\chi^{(3)}|$ were determined at respective fundamental photon energies, following the procedure as we reported previously.[16,17]

III. RESULTS AND DISCUSSIONS

A. Linear and nonlinear optical spectra of polysilanes

The one- (solid curves) and two-photon absorption spectra (dashed curves) for respective PS's are shown in Fig. 1. The peaks in the one- and two-photon spectra correspond to the lowest ($\nu=1$) dipole-allowed exciton and the second lowest ($\nu=2$) dipole-forbidden exciton. Several important experimental parameters are listed in Table I. As seen in Fig. 1 and the upper part of Table I, it is clear that the energies of the lowest and the second lowest excitons are both considerably dependent on the backbone conformation. The E_1 energy is smallest in the transplanar PDHS, but it increases in the order of the alternating transgauche PDTDS, 7/3 helical PDBS, and disordered PMMPS. According to the band structure calculation,[36–38] the alternation of E_1 results from the change in the electronic structure of backbone chains, mainly due to difference in the bandwidth of the highest occupied valence band (HOVB) and the lowest unoccupied conduction band (LUCB), as discussed later in Sec. III C.

In Fig. 2, the modulus $|\chi^{(3)}|$ spectra obtained from the

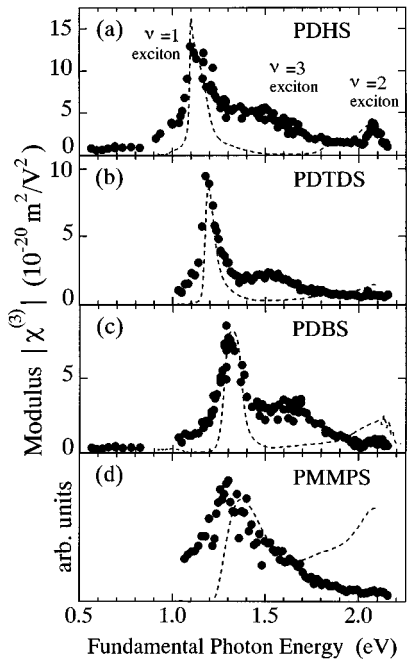

FIG. 2. Modulus of complex third-order nonlinear optical susceptibility $\chi^{(3)}(-3\omega;\omega,\omega,\omega)$ vs fundamental photon energy $\hbar\omega$ for four kinds of PS's, (a) PDHS, (b) PDTDS, (c) PDBS, and (d) PMMPS (filled circles), against the fundamental photon energy $\hbar\omega$. The absorption spectra (dashed curves) are plotted against three-photon energy for comparison. The main peak, due to three-photon resonance to the lowest ($\nu=1$) exciton, and the shoulderlike structure, due to three-photon resonance to the third ($\nu=3$) exciton, are clearly observed in PDHS, PDTDS, and PDBS.

THG measurements are plotted for four kinds of PS's by filled circles against the fundamental photon energy $\hbar\omega$ in eV. The one-photon absorption spectra are also plotted by dashed curves where the incident photon energy should be taken just three times as much as the fundamental photon energy. As clearly seen, the shapes of NLO spectra for the respective PS's are quite similar to each other, except for PMMPS. The main peaks of $|\chi^{(3)}|$ spectra are located at 1.09 eV for PDHS, 1.18 eV for PDTDS, 1.31 eV for PDBS, and 1.35 eV for PMMPS, which are obviously attributable to the three-photon resonance structure to the lowest ($\nu=1$) dipole-allowed excitons. We call them hereafter the first peaks. In PDHS, a small but distinct peak is observed at 2.10 eV. This peak is attributed to the two-photon resonant structure to the second ($\nu=2$) dipole-forbidden exciton, since the energy (2.1 eV) coincides well with half of the second ($\nu=2$) exciton energy (4.19 eV), obtained from two-photon absorption spectra shown in Fig. 1(a). The corresponding peaks in the $|\chi^{(3)}|$ spectra of other three PS's could not be detected, because the range of THG measurements was limited up to 2.2 eV, which is short of reaching the two-photon resonant peaks expected at around 2.23 eV in PDTDS and 2.38 eV in PDBS.

Between the three- and two-photon resonance peaks of PDHS, there is a broad structure at around 1.5 eV. Similar structures are also observed in PDTDS and PDBS at energies which are 0.3–0.4 eV higher than the first peaks. We have assigned this feature to the three-photon resonance to the one-photon-allowed (two-photon-forbidden) third ($\nu=3$) exciton (with possible contribution of nearby higher bound or unbound exciton states), which are located at energy about 1 eV higher than the lowest exciton.[16,17] Such dipole-allowed exciton states are not observable in the ordinary linear (one-photon) absorption spectra for the reason mentioned above, and become observable only in the THG $|\chi^{(3)}|$ spectra, in which the multiphoton nonlinear optical processes between excitons are playing an essential role, as previously discussed in detail for PDHS.[16,17,23,24]

In contrast, PMMPS displays a qualitatively different behavior. First, the second peak was not clearly observed in the NLO spectra. Second, the linear absorption spectrum is rather broad as compared with sharp peaks in other PS's, as seen in Fig. 1. Third, the peak energy of THG $|\chi^{(3)}|$ spectrum is slightly lower than the one-third of the one-photon exciton absorption peak energy. These features are likely attributable to the backbone disorder effect. Therefore, we shall omit the result of PMMPS from the following discussions.

B. Characteristic parameters for excitons in polysilanes

In order to make quantitative discussion on the exciton states in PS's, we shall introduce two key parameters, both derived directly from the experimental linear and nonlinear optical spectra. But before defining these parameters, it will be better to start the discussion with a remark on the lowest exciton energy E_1 under the influence of the conformational change. The E_1 value changes from about 3.3 eV (PDHS) to 4.0 eV (PDBS), depending on the Si-backbone conformation. Although the E_1 value may be effected by several factors, the most dominant one is thought to be the change in the bandwidths of HOVB and LUCB, judging from the theoretical band calculations.[36–38] Further support is also given below (Sec. III C), where the exciton biding energy is rather insensitive to the backbone conformations, so that the E_1 value is predominantly determined by the band-gap energy, or equivalently by the bandwidths of σ-bonding HOVB and σ^*-antibonding LUCB.

The important parameters obtained directly from the one-photon, two-photon, absorption, and THG $|\chi^{(3)}|$ spectra are the relative positions of the lowest, the second, and the third exciton energies E_1, E_2, and E_3 for PDHS, PDTDS, and PDBS. The results are summarized in Fig. 3, as a function of the E_1 value in the respective PS's. An interesting feature is that the energy difference between the lowest and second excitons, $\Delta E_{12}=E_2-E_1$, remains almost constant (about 0.8–0.9 eV) in these PS's, though the respective energies shift by about 0.65 eV in these series. According to the Wannier exciton picture, the binding energies of the lowest and second excitons are represented as $\Delta E(\nu=1)=E_g-E_1$ and $\Delta E(\nu=2)=E_g-E_2$, where E_g is the band-gap energy. Hence, $\Delta E_{12}=\Delta E(\nu=1)-\Delta E(\nu=2)$ is equal to the difference of the binding energy of the lowest and second excitons.

Another important experimental parameter is the relative magnitude of the third-order optical nonlinearity, which is defined by $|\chi^{(3)}|/\alpha$. Here the THG $|\chi^{(3)}|$ value is divided by the absorption coefficient α in the three-photon resonance region of the first peaks. This particular parameter has been used as the figure of merit for the conventional evaluation for nonlinear optical materials. In the case of PS's, the optical nonlinearity is dominated by the exciton transitions, and,

from the reasoning mentioned below, we may regard $|\chi^{(3)}|/\alpha$ as a characteristic parameter related to the exciton Bohr radius a_B. The linear (one-photon) optical susceptibility $\chi^{(1)}_{\mathrm{OP}}$, and the nonlinear optical susceptibility $\chi^{(3)}_{\mathrm{THG}}$ for THG are respectively represented as follows:

$$\chi^{(1)}_{\mathrm{OP}}=\frac{N}{3\varepsilon_0}\sum_n \langle g|\mu|a\rangle\langle a|\mu|g\rangle\cdot\left(\frac{1}{E_a-E-i\Gamma_a}+\frac{1}{E_a+E+i\Gamma_a}\right), \tag{1}$$

and

$$\chi^{(3)}_{\mathrm{THG}}=\frac{N}{6\varepsilon_0}\sum_{a,f,a'}\langle g|\mu|a'\rangle\langle a'|\mu|f\rangle\langle f|\mu|a\rangle\langle a|\mu|g\rangle \times\left[\frac{1}{(E_{a'}-3E-i\Gamma_{a'})(E_f-2E-i\Gamma_f)(E_a-E-i\Gamma_a)}+\frac{1}{(E_{a'}+E+i\Gamma_{a'})(E_f+2E+i\Gamma_f)(E_a+3E+i\Gamma_a)}+\frac{1}{(E_{a'}+E+i\Gamma_{a'})(E_f-2E-i\Gamma_f)(E_a-E-i\Gamma_a)}+\frac{1}{(E_{a'}+E+i\Gamma_{a'})(E_f+2E+i\Gamma_f)(E_a-E-i\Gamma_a)}\right]. \tag{2}$$

Here N is the unit cell density, g is the ground state, a and a' are the dipole-allowed exciton (ν=odd) states, f is a dipole-forbidden exciton (ν=even) state, $\langle i|\mu|j\rangle$ is the dipole matrix moment between the i and j excitons ($i,j=g,a,a',f$), E is the incident photon energy, and E_i and Γ_i are the energy and damping constant of the exciton state i, respectively. If we take $|\chi^{(3)}|$ at the three-photon resonance region for THG ($3E=E_1$) and $\chi^{(1)}_{\mathrm{OP}}$ at the absorption peak ($E=E_1$), we find the ratio $|\chi^{(3)}|/\alpha$ is approximately proportional to $\langle 1|\mu|f\rangle\langle f\mu|1'\rangle$, according to Eqs. (1) and (2). Among various terms in Eq. (2) for different f, the dominant contribution obviously comes from the terms which includes $\langle 1|\mu|2\rangle$. In the Wannier exciton regime, it is easy to show that $\langle 1|\mu|2\rangle$ is nearly proportional to the exciton Bohr radius a_B. In the case of the 1D exciton, $|\chi^{(3)}|/\alpha$ is shown to depend on the exciton Bohr radius as $|\chi^{(3)}|/\alpha\sim(a_B)^6$ in the weak coupling limit (i.e., the Wannier exciton regime), as discussed later in Sec. III D.

In the early stage of study, the optical nonlinearity was interpreted in terms of a simple band model without taking account of the exciton effect,[39,40] leading to a well-known relation; $\chi^{(3)}\sim(1/E_g)^6$, E_g being the band-gap energy. However, in the exciton-dominated case, it is more meaningful to adopt the ratio $|\chi^{(3)}|/\alpha$ for the experimental evaluation of nonlinear optical response. The reasons may be summarized as follows: First, the experimental $|\chi^{(3)}|$ values should be corrected for the polymer density in order to evaluate the optical nonlinearity per each unit of polymers. Since both $|\chi^{(3)}|$ and α are proportional to the polymer density N, the $|\chi^{(3)}|/\alpha$ becomes independent of the polymer density. Second, both the $|\chi^{(3)}|$ and α values are measured on film samples where the experimental errors are apt to be introduced in the evaluation of the film thickness d. By taking the ratio $|\chi^{(3)}|/\alpha$, the error in d is canceled out, since both of experimental values are proportional to d. Third, in order to make comparison between the THG $|\chi^{(3)}|$ values for different PS's, we have to take account of the fact that the spectral widths of the resonant structures is considerably dependent on the film quality. In such a case, the ratio $|\chi^{(3)}|/\alpha$ becomes a more meaningful quantity than the $|\chi^{(3)}|$ values themselves, since both one-photon (absorption) and three-photon (THG $|\chi^{(3)}|$) resonance spectra for respective PS's are subject to the same damping effect as seen in Fig. 2.

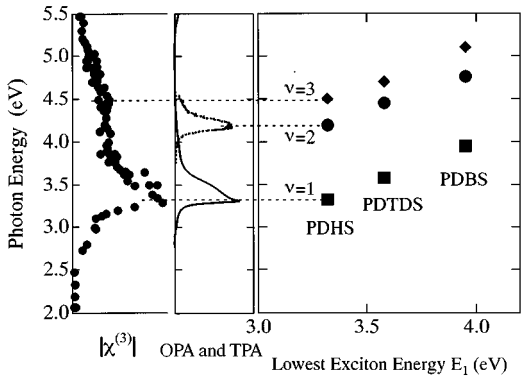

FIG. 3. The lowest, second, and third exciton energies of PDHS, PDTDS, and PDBS, vs the lowest exciton energy evaluated from one-photon absorption, two-photon absorption, and THG $|\chi^{(3)}|$ spectra, respectively. These exciton energies depend on the backbone conformation.

Several important parameters including the $|\chi^{(3)}|/\alpha$ values are assembled altogether in Table I. It is worth noting that the $|\chi^{(3)}|/\alpha$ value decreases as the E_1 value decreases, in contrast with nearly E_1-independent ΔE_{12} values, as shown in Fig. 4. The latter result suggests that the exciton binding energy is insensitive to the backbone structure. In the following discussions, we shall consider characteristic nature of the Q1D exciton states in PS's, first by showing the limited validity of the 1D Wannier exciton model and then by present-

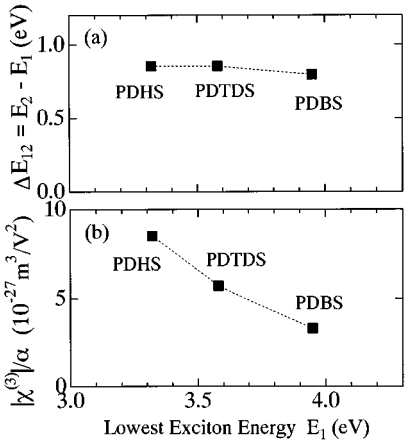

FIG. 4. (a) Energy difference between the lowest and the second excitons, $\Delta E_{12}=E_2-E_1$, vs the lowest exciton energy E_1. (b) $|\chi^{(3)}|/\alpha$ vs the lowest exciton energy E_1. $|\chi^{(3)}|/\alpha$ decreases with increasing E_1, whereas E_2-E_1 remains almost constant.

ing a more general treatment using a 1D tight-binding model supplemented by the long-range Coulomb interactions.

C. Limited validity of the Wannier exciton model

In previous papers,[16,17] we interpreted the linear and nonlinear optical spectra of PDHS in terms of the Q1D Wannier exciton model. The starting point of the Wannier exciton picture is the one-electron band structure, including the band gap and the effective masses of electrons and holes. According to *ab initio* band-structure calculations,[37,38] the electron and hole effective masses for trans-planar polysilane are considerably smaller than those for gauche-helix polysilane. The reason is that the transfer energy between neighboring (intrachain) σ-bonds depends strongly on the coplanarity of σ-bonds and hence on the backbone conformation. As a result, the one-electron bandwidths for the conduction and valence bands become considerably large for trans-planar polysilane as compared with gauche-helix polysilane. Considerable differences in the electron and hole masses are thus predicted for different conformations, for instance, electron effective mass of about 0.104 for trans-planar polysilane and 1.45 for gauche-helix polysilane.[37]

The observed E_1 value increases in the sequence of PDHS, PDTDS, PDBS, and PMMPS, which is in accord with the predicted trend of the bandwidths decreasing in the same sequence. Consequently, we may regard the E_1 value as the experimental parameter representing the relative magnitude of effective mass.

Now we shall proceed to examine whether the Wannier exciton picture works well to interpret the results shown in Fig. 4. At first, we shall investigate the case for $|\chi^{(3)}|/\alpha$ shown in Fig. 4(b). According to the Wannier exciton picture for Q1D semiconductors,[11] the effective exciton Bohr radius (a_B) is given by $a_B=4\pi\varepsilon\hbar^2/\mu e^2$. Since the effective reduced mass μ is approximately inversionally proportional to the bandwidths a_B will be proportional to the bandwidths of HOVB and LUCB in PS's. This leads to a prediction that the exciton Bohr radius shrinks as the lowest exciton energy E_1 increases. The result shown in Fig. 4(b), where the $|\chi^{(3)}|/\alpha$ value decreases with the increase of E_1, is in accord with this Wannier exciton picture, as long as the magnitude of the NLO response is concerned.

Next, we shall examine the trend of ΔE_{12} mentioned in Sec. III B. According to the Wannier exciton picture for the 3D and 2D excitons, the exciton binding energies are proportional to the effective reduced mass μ, leading to the prediction that the ΔE_{12} value is also proportional to μ. But in the Q1D system, such a simple relation is hardly expected, due to the singularity of the electron-hole interaction at the origin. The actual potential is usually simulated by a truncated Coulomb potential $V(x)$ having a cusp-type cutoff at the origin.[14]

As a model of $V(x)$, the following cusp-type cutoff Coulomb potential has been adopted here for the calculation:

$$V(x)=\frac{e^2}{4\pi\epsilon(|x|+x_0)}. \tag{3}$$

Here ε is the effective dielectric constant, and x_0 is the cutoff parameter. The calculated binding energy $\Delta E^{1D}(\nu=1)$ and $\Delta E^{1D}(\nu=2)$ are shown in Fig. 5 by solid curves as a function

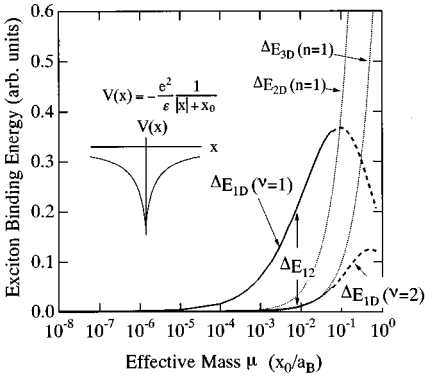

FIG. 5. Calculated exciton binding energies of Wannier-type lowest $[\Delta E_{1D}(\nu=1)]$ and second $[\Delta E_{1D}(\nu=2)]$ excitons in 1D semiconductors as a function of the effective mass (solid curves) in the case of Coulomb potential with a cusp-type cutoff at the origin (shown in the inset). Calculated exciton binding energies in case of 2D and 3D semiconductors, $\Delta E_{2D}(n=1)$ and $\Delta E_{3D}(n=1)$ are also shown by dotted curves for comparison.

of the effective reduced mass μ in units of x_0/a_B. As seen in this figure, $\Delta E^{1D}(\nu=1)$, $\Delta E^{1D}(\nu=2)$, and ΔE_{12} $[=\Delta E^{1D}(\nu=1)-\Delta E^{1D}(\nu=2)]$ do increase with increasing μ, except the region shown by dashed curves where the ratio x_0/a_B becomes larger than 0.06.[41]

According to the calculations, the ΔE_{12} value is also predicted to increase with μ. This is evidently in contradiction to the experimental result shown in Fig. 4(a). To summarize, we have shown that the Wannier exciton (i.e., the effective-mass approximation) picture can explain the trend of $|\chi^{(3)}|/\alpha$, but is in contradiction to the trend of ΔE_{12}. A consistent picture is given only by taking account of a suitable admixture of the Wannier and the Frenkel excitons, as discussed in Sec. III D.

D. Approach from an intermediate exciton theory

Now, let us examine the same problem as discussed in Sec. III C by using a 1D exciton model developed by Abe and co-workers.[23,24,42,43] In this treatment, exciton states are dealt with by a 1D tight-binding model supplemented by long-range Coulomb interactions, where an intermediate character between the Frenkel and Wannier regimes can be treated, in contrast with the standard Wannier exciton picture based on the simple one-electron band model discussed in Sec. III C.

The essential procedure of this treatment is as follows: As a first step, the Sandorfy *C* model is used as the one-electron Hamiltonian. Two sets of sp^3 orbitals of each Si atoms in the main chain are utilized as the basis set. The transfer energy between the overlapping sp^3 orbital protruded from adjacent Si atoms are represented as t_ν, while the transfer energy between the two sp^3 orbitals protruded from the same Si atom as t_g. Then, the one-electron Hamiltonian H_0 is expressed as

$$H_0=-t_g\sum_{i,s}\ (C^+_{i,a,s}C_{i,b,s}+\text{H.c.})$$

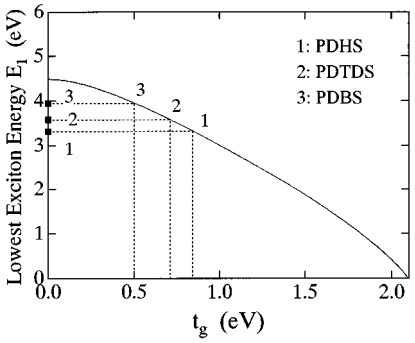

FIG. 6. Calculated lowest exciton energy E_1 as a function of t_g by a 1D exciton model. Experimental E_1 for PDHS, PDTDS, and PDBS are also plotted by filled squares. Here parameters, U, V, and t_ν are fixed at 4.9, 2.45, and 2.1 eV, respectively.

$$-t_\nu \sum_{i,s} (C^+_{i,a,s} C_{i-1,b,s} + \text{H.c.}). \tag{4}$$

Here $C^+(C)_{i,a,s}$ and $C^+(C)_{i,b,s}$ denote the creation (annihilation) operators for the respective sp^3 orbital (denoted as a and b) of Si atom at the site i with the spin s, H.c. being the Hermitian conjugate. After the diagonalization under the periodic boundary condition, the one-electron conduction and valence bands are obtained, both having a bandwidth of $2t_g$, with a band-gap energy of $2(t_\nu - t_g)$. Finally, the Coulomb interaction H_{e-e} is included by the following expression:

$$H_{e-e} = U \sum_{i,\mu} C^+_{i,\mu,\uparrow} C_{i,\mu,\uparrow} C^+_{i,\mu,\downarrow} C_{i,\mu,\downarrow} + \tfrac{1}{2} \sum_{\substack{i,\mu,s \\ (i,\mu)\neq(j,\mu')}} \sum_{j,\mu',s'} V_{i,\mu;j,\mu'} C^+_{i,\mu,s} C_{i,\mu,s} C^+_{j,\mu',s'} C_{j,\mu',s'}, \tag{5}$$

where U is the on-site Coulomb energy, and $V_{i,\mu;j,\mu'}(i \neq j) = V/|i-j|$, V being a constant. When an electron is excited from the valence to the conduction bands, the excited states are obtained by the diagonalization of the total Hamiltonian within the single excitation from the ground state, leading to proper bound and unbound 1D exciton states in this regime. Numerical calculation of these exciton states has been performed using a cyclic 1D system composed of 400 sites (the number of Si atoms is 200).

We have assumed the following approximations for a PS system having three kinds of backbone conformation: (1) The bandwidth is predominantly determined by the parameter t_g, while t_ν plays a minor role. This assumption should be reasonable from considerations mentioned in Sec. III C. (2) The following electronic parameters are assumed to be constant: $U=4.90$ eV, $V=2.45$ eV, and $t_\nu=2.10$ eV for all the PS's under discussion, an assumption which seems to hold for actual PS systems under consideration. The lowest exciton energy E_1 calculated as a function of t_g is shown in Fig. 6. Note that the E_1 value decreases as t_g increases, or equivalently as the one-electron band-gap energy $2(t_\nu - t_g)$ decreases. According to this model, the parameter t_g is a single parameter, by which the observed trend of experimental parameters $E_1, E_2, \Delta E_{12}$, as well as $|\chi^{(3)}|/\alpha$ ought to be explained in a consistent way. Following this conjecture, we have estimated the t_g values of respective PS's from a plot of Fig. 6, where the experimental E_1 values for three kinds of PS's are shown by filled squares on the ordinate. It leads to a estimation that $t_g=0.84$ eV for PDHS, 0.71 eV for PDTDS, and 0.50 eV for PDBS, respectively. The remaining parameters U, V, and t_ν have been determined so that the calculated parameters $|\chi^{(3)}|/\alpha$ and ΔE_{12} are best fitted with the experimental data (which will be shown by solid curves in Figs. 9 and Fig. 10).

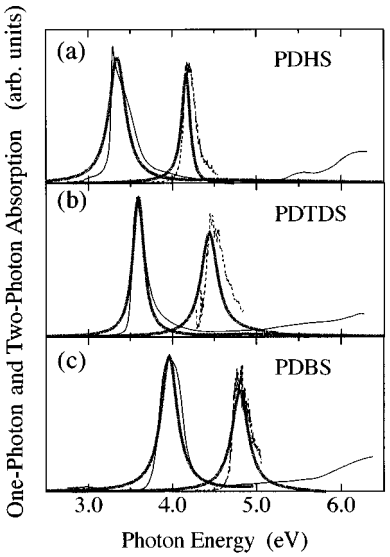

FIG. 7. Experimental one-photon (thin solid curves) and two-photon absorption (thin dashed curves) spectra for PDHS, PDTDS, and PDBS in comparison with the calculated spectra (dotted curves), by the 1D exciton model. Parameters used for the calculation are shown in Table II.

The details of theoretical procedure are the same as described in previous works,[42,43] and we first show the calcu-

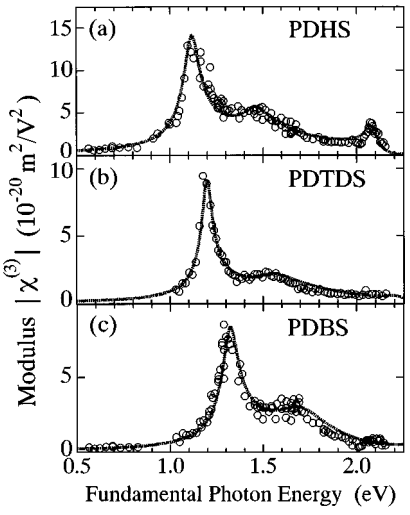

FIG. 8. Experimental THG $|\chi^{(3)}|$ spectra (open circles) for PDHS, PDTDS, and PDBS in comparison with the calculated spectra (dotted curves), by the 1D exciton model. Parameters used for the calculation are shown in Table II.

TABLE II. Some important parameters used for calculation of theoretical linear and nonlinear optical spectra (Figs. 7 and 8) by the one-dimensional exciton model.

Parameters (units in eV)	PDHS	PDTDS	PDBS
U	4.9	4.9	4.9
V	2.45	2.45	2.45
t_v	2.1	2.1	2.1
t_g	0.84	0.71	0.5
$\Gamma(\nu=1)$	0.12	0.08	0.12
$\Gamma(\nu=2)$	0.06	0.12	0.12
$\Gamma(\nu=3)$	0.18	0.28	0.36

lated results for one- and two-photon absorption spectra in Fig. 7 and for $|\chi^{(3)}|$ spectra in Fig. 8. In these calculations, all the parameters used are listed in Table II, including the damping constants $\Gamma(\nu=1, 2, \text{and } 3)$ for the respective exciton transitions. Agreement between the experimental and calculated spectra is satisfactory, in support of the good consistency of the present model.

On the basis of these results, we then proceed to a discussion of the implication of exciton parameters in the NLO process in PS's. In Fig. 9(a), calculated curves for $|\chi^{(3)}|/\alpha$ are plotted by solid curves on a logarithmic scale, as a function of E_1. The filled squares represent the experimental E_1 values for PDHS, PDTDS, and PDBS, respectively. A part of the region in which the experimental points are included is shown in Fig. 9(b) on an expanded scale. In Fig. 10(a), the calculated ΔE_{12} curve is plotted against E_1 together with the experimental points shown by filled squares. A part of the plot in Fig. 10(a) is shown in an expanded scale as in Fig. 9. It is worth noting that the experimental trends shown in Fig. 4 for ΔE_{12} and $|\chi^{(3)}|/\alpha$ are well reproduced by the present calculations. This is clearly in contrast to the simple Wannier exciton picture, where ΔE_{12} shows a monotonous increase

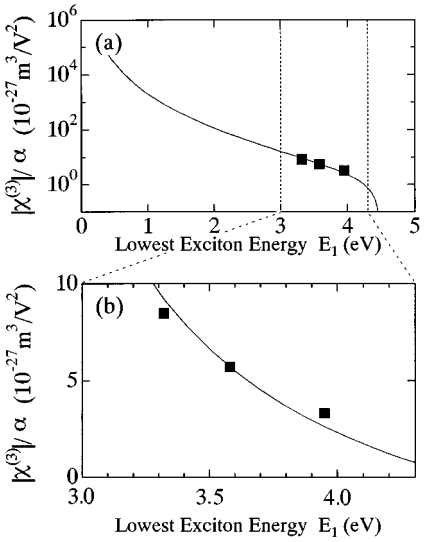

FIG. 9. Experimental $|\chi^{(3)}|/\alpha$ (filled squares) for PDHS, PDTDS, and PDBS, plotted against the lowest exciton energy E_1, in comparison with the theoretical results (solid curves). A part of (a) is expanded in (b).

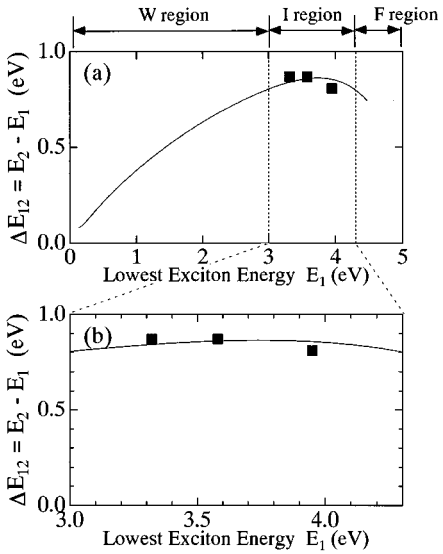

FIG. 10. Experimental $\Delta E_{12}=E_2-E_1$ for PDHS, PDTDS, and PDBS, plotted against the lowest exciton energy E_1, in comparison with the calculation (solid curves). A part of (a) is expanded in (b). A sublinear behavior of $\Delta E_{12}=E_2-E_1$ on E_1 is observed when E_1 is larger than 3.8 eV.

with increasing of E_1 (see Fig. 5). Although these calculations involve the parameter fitting procedure for U, V, and t_g, it should be noted that the features are essentially the same for different sets of values for U, V, and t_ν, provided that $U=2V$. The final choice of the U, V, and t_ν values was achieved so as to get the best fit between the calculated and the experimental results as a whole.

E. Intermediate character of excitons in polysilanes between the Wannier and Frenkel regimes

The unique character of Q1D exciton states in PS's is that their characteristic optical features, revealed by linear and nonlinear spectroscopy, cannot be explained in a consistent way by either Wannier or Frenkel-type pictures. Rather, the nature of their excitons should be interpreted by a picture of ''intermediate (I) exciton'' in between the Wannier (W) and the Frenkel (F) regimes. In Fig. 10, we indicated an area denoted the I region, which is located between the W region and the F region, as shown in Fig. 10(a).

It is illustrative to see the spatial extension of exciton as a function of the lowest exciton energy E_1 in Fig. 11. In the small E_1 region ($E_1<3$ eV) the exciton Bohr radius is larger than several lattice constants. This region has a character of the Wannier exciton, so we shall refer this region as the W region. In contrast, in the region of larger E_1 ($E_1=3$–4 eV), the Bohr radius becomes as small as a few lattice constants. This region corresponds to the I region in Fig. 10(a). Such a localized exciton can no longer be regarded as a Wannier-type one, and comes to show an intermediate character between Wannier and Frenkel regimes. In the limit of $t_g=0$ in the F region, the lowest exciton is localized only at a single site, surely corresponding to the Frenkel-limit excitons, where the photogenerated electron and hole exist only at the same site. In contrast, in the second lowest and third lowest

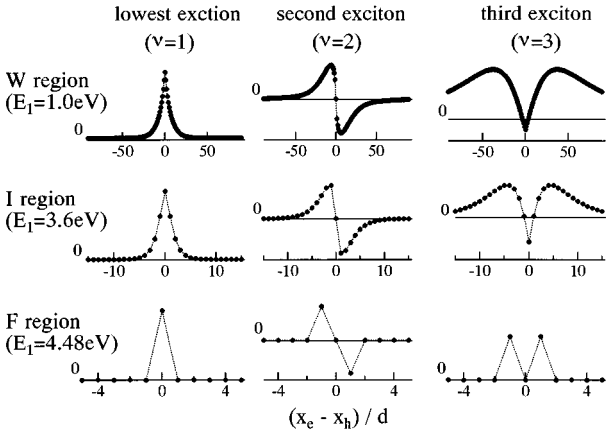

FIG. 11. Calculated exciton envelope functions for the lowest ($\nu=1$), second ($\nu=2$), and third ($\nu=3$) excitons in the three typical regions: *W* (Wannier), *I* (intermediate), and *F* (Frenkel) regions.

excitons, the envelope functions spread over three sites with nodes at the center, corresponding to the antisymmetric and symmetric charge-transfer excitons, respectively, as shown in Fig. 11.

The unusual behavior of the separation of the lowest exciton and the second exciton energy, ΔE_{12}, as discussed above, can be regarded as a manifestation of intermediate character between the Frenkel and Wannier regimes, especially due to the effect of on-site correlation U. To clarify the effect of on-site correlation U on the behavior of ΔE_{12}, results for the same calculation on the spin-singlet and spin-triplet excitons are presented for various values of U in Fig. 12. In the case of a singlet exciton, an unusual behavior becomes apparent when U becomes large. However, such a behavior is not seen for the triplet exciton, strongly supporting the above speculations.

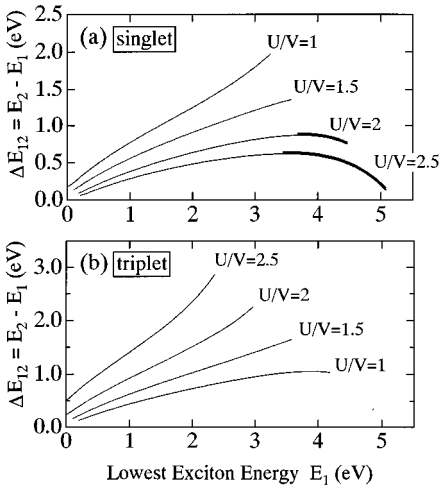

FIG. 12. Dependence of $\Delta E_{12}=E_2-E_1$ on E_1 in the case of (a) spin-singlet and (b) spin-triplet excitons, calculated for various values of on-site Coulomb energy U: $U/V=1$, 1.5, 2, and 2.5. Note that the sublinear behavior of ΔE_{12} for the former is observed when $U/V=2$ or 2.5 ($U/V>1.7$), [thick solid curves], whereas such behavior is not observed in the case of triplet exciton.

As the final remark, we shall mention the physical implications of increasing $\Delta E_{12}=E_2-E_1$ with decreasing E_1 in the Frenkel regime shown by the curves for $U/V=2$ and 2.5 in Figs. 10(a) and 12(a). Such a characteristic feature can be attributed to the perturbation on the excitons by t_g in the Frenkel-limit regime, where respective excitons are represented by Frenkel or charge-transfer excitons, as shown in Fig. 11. In the present case, the transfer energy T_g between adjacent σ bonds is written as

$$T_g=-t_g\sum_{i,\sigma}(C^{+}_{i,a,\sigma}C_{i,b,\sigma}+\text{H.c.}). \tag{6}$$

By this symmetric perturbation, mixing occurs between the lowest ($\nu=1$) and third ($\nu=3$) excitons, whereas the antisymmetric charge-transfer exciton ($\nu=2$) is mixed with higher odd exciton states. As a result, the lowest exciton energy E_1 decreases by an amount δE_1 given by

$$\delta E_1=\frac{|\langle 3\text{rd exc.}|T_G|1\text{st exc.}\rangle|^2}{E_3-E_1}=\frac{2t_g^2}{E_3-E_1}. \tag{7}$$

Likewise, the second exciton level is shifted downward due to the dominant mixing with the fourth exciton by δE_2 given by

$$\delta E_2=\frac{|\langle 4\text{th exc.}|T_G|2\text{nd exc.}\rangle|^2}{E_4-E_2}=\frac{t_g^2}{E_4-E_2}. \tag{8}$$

Hence, when the E_1 value becomes large and an inequality relation $E_1>E_3-2(E_4-E_2)$ comes to hold, $\Delta E_{12}=E_2-E_1$ increases in the large-E_1 region with an increase of the transfer energy t_g, as demonstrated in Fig. 10(a). This situation corresponds to the Frenkel regime, where the lowest exciton binding energy is limited by the on-site electron repulsion, that is, by the exchange interaction effect.

IV. CONCLUSIONS

In conclusion, the characteristic features of Q1D exciton states in PS's have been elucidated by means of systematic studies on PS's having various backbone conformations. In the polymeric semiconductors like PS's, the exciton effect becomes remarkable, so that a simple Wannier exciton picture can no longer be applied to the exciton states. Instead, the intermediate exciton picture—that is, an admixture of Wannier and Frenkel exciton characters—has to be taken into account, where the on-site Coulomb energy comes to play a crucial role in determining the exciton structures which are responsible for many interesting nonlinear optical properties.

One of the most notable points in the experimentally observed features is that the $|\chi^{(3)}|/\alpha$ increases, but the energy difference ΔE_{12} remains almost unchanged, as the lowest exciton energy decreases. Quite similar features have been also observed in the π-conjugated polymer polydiacetylenes

(PDA's), leading to a significant difference in the nonlinear optical spectra of blue- and red-form PDA's.[44,45]

ACKNOWLEDGMENTS

This work was carried out partly in collaboration with H. Sunamura, A. Makimoto, and S. Yasukawa (University of Tokyo), and Dr. H. Kobayashi and Dr. K. Kubodera (NTT Optoelectronic Lab.). We are also grateful to Professor S. Abe (ETL, Tsukuba University), Professor K. Miyano (University of Tokyo), Professor T. Ogawa (Osaka City University), and Professor T. Tokihiro (University of Tokyo) for their enlightening discussions.

[1] R. Cingolani, M. Lepore, R. Tommasi, I. M. Catalano, H. Lage, D. Heitmann, K. Ploog, A. Shimizu, H. Sakaki, and T. Ogawa, Phys. Rev. Lett. **69**, 4910 (1993).

[2] H. Ando, H. Oohashi, and K. Kanbe, J. Appl. Phys. **70**, 7024 (1991).

[3] H. Akiyama, S. Koshiba, T. Someya, K. Wada, H. Noge, Y. Nakamura, T. Inoshita, A. Shimizu, and H. Sakaki, Phys. Rev. Lett. **72**, 924 (1994).

[4] *Nonlinear Optical Properties of Organic Molecules and Crystals*, edited by D. S. Chemla and J. Zyss (Academic, Orlando, FL, 1987), Vol. 2.

[5] *Nonlinear Optical Effects in Organic Polymers*, edited by J. Messier, F. Kajzar, P. Prasad, and D. Ulrich (Kluwer Academic, Dordrecht, 1989).

[6] *Relaxation in Polymers*, edited by T. Kobayashi (World Scientific, Singapore, 1993).

[7] S. Etemad *et al.*, in *Molecular Nonlinear Optics*, edited by J. Zyss (Academic, New York, 1994).

[8] R. D. Miller and J. Michl, Chem. Rev. **89**, 1359 (1989).

[9] *Silicon Based Polymer Science*, edited by J. M. Zeigler and F. W. G. Fearson, Advances in Chemistry Series Vol. 224 (American Chemical Society, Washington, D. C., 1990).

[10] R. G. Kepler and Z. G. Soos, in *Relaxation in Polymers*, edited by T. Kobayashi (World Scientific, Singapore, 1993).

[11] R. Loudon, Am. J. Phys. **27**, 649 (1959).

[12] R. J. Elliot and R. Loudon, J. Phys. Chem. Solids **15**, 196 (1960).

[13] S. Abe, J. Phys. Soc. Jpn. **58**, 62 (1989).

[14] T. Ogawa and T. Takagahara, Phys. Rev. B **43**, 14 325 (1991).

[15] T. Ogawa and T. Takagahara, Phys. Rev. B **44**, 8138 (1991).

[16] T. Hasegawa, Y. Iwasa, H. Sunamura, T. Koda, Y. Tokura, H. Tachibana, M. Matsumoto, and S. Abe, Phys. Rev. Lett. **69**, 668 (1992).

[17] T. Hasegawa, Y. Iwasa, T. Koda, H. Kishida, Y. Tokura, S. Wada, H. Tashiro, H. Tachibana, M. Matsumoto, and R. D. Miller, in Light Emission from Novel Silicon Materials, edited by Y. Kanemitsu, M. Kondo, and K. Takeda [J. Phys. Soc. Jpn. Suppl. B **63**, 64 (1994)].

[18] J. R. G. Thorne, Y. Ohsako, J. M. Zeigler, and R. M. Hochstrasser, Chem. Phys. Lett. **162**, 455 (1989).

[19] Z. G. Soos and R. G. Kepler, Phys. Rev. B **43**, 11 908 (1991).

[20] T. Hasegawa, Y. Iwasa, H. Kishida, T. Koda, Y. Tokura, H. Tachibana, and Y. Kawabata, Phys. Rev. B **45**, 6317 (1992).

[21] H. Kishida, T. Hasegawa, Y. Iwasa, T. Koda, Y. Tokura, H Tachibana, M. Matsumoto, S. Wada, T. T. Lay, and H. Tashiro, Phys. Rev. B **50**, 7786 (1994).

[22] H. Tachibana, Y. Kawabata, S. Koshihara, and Y. Tokura, Solid State Commun. **75**, 5 (1990).

[23] S. Abe, M. Schreiber, and W.-P. Su, Chem. Phys. Lett. **192**, 425 (1992).

[24] S. Abe, J. Phys. Soc. Jpn. Suppl. B **63**, 56 (1994).

[25] B. S. Hudson, B. R. Kohler, and K. Schulten, in *Excited States*, edited by E. C. Lim (Academic, New York, 1982), Vol. 6.

[26] Z. G. Soos, P. C. M. McWilliams, and G. W. Hayden, Chem. Phys. Lett. **171**, 14 (1990).

[27] S. N. Dixit, Danda Guo, and S. Mazumdar, Phys. Rev. B **43**, 6781 (1991).

[28] H. Tachibana, M. Matsumoto, Y. Tokura, Y. Moritomo, A. Yamaguchi, S. Koshihara, R. D. Miller, and S. Abe, Phys. Rev. B **47**, 4363 (1993).

[29] Y. Moritomo, Y. Tokura, H. Tachibana, Y. Kawabata, and R. D. Miller, Phys. Rev. B **43**, 14 746 (1991).

[30] Y. Tokura, H. Tachibana, H. Kishida, Y. Moritomo, and M. Matsumoto, [J. Phys. Soc. Jpn. Suppl. B **63**, 30 (1994)].

[31] S. Wada, H. Tashiro, Y. Urata, Thi Thi Lay, A. Kasai, and K. Toyota, Appl. Phys. B **57**, 435 (1993).

[32] K. Kuodera and H. Kobayashi, Mol. Cryst. Liq. Cryst. **182A**, 103 (1990).

[33] F. Kajzar, J. Messier, and C. Rosilio, J. Appl. Phys. **60**, 3040 (1986).

[34] F. Kajzar and J. Messier, Phys. Rev. A **32**, 2352 (1985).

[35] For PMMPS, the thickness measurement was not successful, as the film is too soft (or oily) to measure the thickness by directly contacting type thickness meter.

[36] J. W. Mintmire, Phys. Rev. B **39**, 13 350 (1989).

[37] K. Takeda, K. Shiraishi, and N. Matsumoto, J. Am. Chem. Soc. **112**, 5043 (1990).

[38] K. Takeda, J. Phys. Soc. Jpn. Suppl. B **63**, 1 (1994).

[39] K. C. Rustagi and J. Ducuing, Opt. Commun. **10**, 258 (1974).

[40] C. Sauteret, J.-P. Hermann, R. Frey, F. Pradere, J. Ducuing, R. F. Baughman, and R. R. Chance, Phys. Rev. Lett. **36**, 956 (1976).

[41] In this particular region [$x_0/a_B > 0.06$; shown by dashed curves for $\Delta E^{1D}(\nu=1)$ and $\Delta E^{1D}(\nu=2)$], the binding energy of the lowest exciton in 2D or 3D semiconductors, $\Delta E^{2D}(n=1)$ and $\Delta E^{3D}(n=1)$ (shown by dotted curves), reaches to and becomes larger than that in 1D semiconductors, which indicates that the assumed cusp-type Coulomb potential approximation fails due to the artifact effect at the origin.

[42] S. Abe, J. Yu, and W.-P. Su, Phys. Rev. B **45**, 8264 (1992).

[43] S. Abe, M. Schreiber, W.-P. Su, and J. Yu, Phys. Rev. B **45**, 9432 (1992).

[44] T. Hasegawa, K. Ishikawa, T. Kanetake, T. Koda, K. Takeda, H. Kobayashi, and K. Kubodera, Chem. Phys. Lett. **171**, 239 (1990).

[45] T. Hasegawa, K. Ishikawa, T. Kanetake, T. Koda, K. Takeda, H. Kobayashi, and K. Kubodera, Synth. Met. **43**, 3151 (1991).